2012 IEEE/RSJ International Conference on
Intelligent Robots and Systems
October 7-12, 2012. Vilamoura, Algarve, Portugal

Catheter Navigation Based on Probabilistic Fusion of Electromagnetic Tracking and Physically-Based Simulation

Alessio Dore[1], Gabrijel Smoljkic[2], Emmanuel Vander Poorten[2], Mauro Sette[2,3], Jos Vander Sloten[2], and Guang-Zhong Yang[1], *Fellow,IEEE*

***Abstract*— Minimally invasive endovascular procedures including robotically assisted intervention require effective intraoperative guidance. This is mainly achieved through intraoperative imaging such as fluoroscopy. Concerns over excessive x-ray radiation and nephrotoxicity due to repeated injection of contrast agents have motivated the development of effective catheter navigation schemes based on limited imaging data. This paper presents a catheter navigation technique based on probabilistic fusion of in situ real-time electromagnetic tracking with physically-based simulation of the mechanical characteristics of the catheter. A catheter with multiple electromagnetic sensors placed along its length has been developed. The sensor data and the catheter insertion-length are used as the boundary condition for determining the shape and position of the catheter within the vasculature. A probabilistic framework based on a Kalman Filter is used to combine the information from the catheter motion algorithm and the electromagnetic tracking data. This provides continuous visualization of the catheter within the lumen without the need of continuous fluoroscopy and contrast injection. The proposed approach has been validated with detailed in vitro experiments demonstrating the potential clinical application of the technique.**

I. INTRODUCTION

During catheter-based endovascular intervention, dexterous manipulation of the guide-wire or catheter through dynamic and complex anatomy of the vasculature is a challenging task. A combination of factors including the difficulty of manipulating the catheter's exact shape and position, as well as the commonly used 2D projection data via subtraction angiograms can all contribute to poor ergonomic control of the device. Furthermore, the limited feedback on the amount of force being applied by the tip of the catheter and of the friction of the catheter to the vessel wall can cause mechanical injury of the endothelial lining of the arterial wall that may initiate platelet aggregation, stimulate neointimal hyperplasia, or even vessel rupture.

To mitigate all these risks, various solutions have been proposed to improve the navigation control of the catheter. Robotic systems have recently been introduced to enhance the precision of the procedure and allow for remote control of the catheterization process away from the scanner. This minimizes the ionizing radiation of the operator whilst at the same time improves the ergonomic control of the device. For example, robotic systems by Hansen Medical Inc. and Sterotaxis aim at obtaining better catheter localization and contact stability [1]. Concepts related to active constraints and autonomous navigation have been explored, but the prerequisite of all these approaches is the accurate determination of the shape of the catheter in relation to the anatomical structure of the vessels. The use of fluoroscopy, particularly with bi-planar or multi-planar imaging setup has the advantage of providing co-registered views of the guide-wire or catheter in relation to the target anatomy. The availability of fluoro-CT further enhances the 3D navigation capability of the procedure. However, concerns over excessive x-ray radiation and nephrotoxicity due to repeated injection of contrast agents have limited the practical deployment of many of the techniques proposed. Advances in XMR integration have alleviated some of the risks mentioned above, but wider applicability of the technique is prohibited by cost and challenges associated with developing fully MR compatible devices. The use of intra-operative ultrasound or OCT (Optical Coherence Tomography) has also been actively pursued. In [2], a probabilistic framework is proposed to detect and track the catheter in 2D angiography images and co-register them with Intravascular Ultrasound (IVUS) images to improve the surgical workflow. A localization method is presented in [3] where the position of the catheter tip is estimated using IVUS images and catheter insertion length. With increasing technical advances and miniaturization of electromagnetic (EM) tracking devices, researchers are also actively pursing real-time tracking-based techniques combined with imaging data to provide effective intraoperative guidance. For example, Shi *et al.* [4] combine IVUS and EM tracking to provide Augmented Reality (AR) visualization to facilitate stent graft deployment. In [5], the position of the tip of a guide-wire is measured with an EM sensor and registered to a CT image to obtain improved localization and reduced use of fluoroscopy. In [6], an EM-based catheter navigation technique is proposed where a virtual endoscopy technique is used to provide a virtual intravascular visual feedback to the surgeon. In parallel to these developments, simulation tools for catheter navigation have also been realized. These models are based on physical characteristics of the catheter with consideration of instrument-tissue interaction. In fact, the same idea has been explored extensively for computerized or robotically assisted needle biopsy [7]. However, thus far

This work was supported by FP7-EU Project "Smart Catheterization (SCATh)"

[1]A. Dore and G.-Z. Yang are with the Hamlyn Centre, Imperial College London, London, UK; e-mail : {a.dore, g.z.yang} at imperial.ac.uk

[2]G. Smoljkic, M. Sette, E. Vander Poorten, and J. Vander Sloten are with the Department of Mechanical Engineering, KU Leuven, Belgium; e-mail : {Gabrijel.Smoljkic, Emmanuel.VanderPoorten, Jos.VanderSloten } at mech.kuleuven.be

[3]M. Sette is with the Institute of Mechatronic Systems, ZHAW, Winterthur, Switzerland; e-mail : mauro.sette at zhaw.ch

catheter-based modeling is mainly used for interventional training platforms. For example, in [8] basic physical laws such as energy minimization and elastic energy are used for developing a guide wire simulation algorithm.

The purpose of this paper is to propose a novel approach that aims at combining an EM tracking for catheter localization with physically-based catheter simulation and modeling based on real-time insertion length measures. A customized design of a catheter with multiple EM sensors has been developed to improve previous EM-based catheter tracking approach by providing measurements of its position and shape. A catheter simulation algorithm is used to predict the catheter motion given a measured insertion length. A Kalman Filter is used to provide a probabilistic framework to fuse these types of information for motion prediction, localization, and shape estimation. Furthermore, the catheter position estimation is registered to the vasculature defined through 3D pre-operative or intra-operative models to provide AR visualization during the procedure with enhanced 3D visualization and navigation risk assessment. The information derived can also be used as the basis for robotically assisted navigation combined with features such as visual servoing and dynamic active constraints. The accuracy of the proposed method has been validated through detailed in-vitro experiments, confirming the effectiveness of the approach.

II. MATERIALS AND METHODS

A. Catheter Representation

During catheter navigation, the operator frequently manipulates and rotates the catheter from the distal end in order to orientate the tip towards the center of the targeted vessel and then pushes it towards the area of interest. This procedure is performed by relying on the catheter shape and position detected from the fluoroscopic imaging data. In this paper, we aim at providing the catheter shape and position with respect to a pre- or intra-operatively acquired 3D model of the vasculature to reduce the use of fluoroscopy.

The catheter is defined by a finite number of oriented points (nodes) $\boldsymbol{x_i} = (x, y, z, \theta, \gamma, \phi)$, where (x, y, z) are the 3D coordinates and (θ, γ, ϕ) are the Euler angles, which are connected by polynomial curves (see Fig. 1) to approximate its shape. The orientation of the points is given by the curve tangent with direction pointing to the tip of the catheter. The points are mapped in the 3D model reference system in order to visualize the catheter inside the vessel and provide the surgeon with necessary visual cues to support the navigation. In order to describe the catheter motion and the associated localization uncertainty, the catheter is represented as a stochastic variable composed by the catheter points $\boldsymbol{x_i}$:

$$\boldsymbol{X}_t = \{\boldsymbol{x}_1, \boldsymbol{x}_2, \ldots, \boldsymbol{x}_n\}_t^T, \tag{1}$$

where n is the number of points used to describe the catheter shape and t is the time.

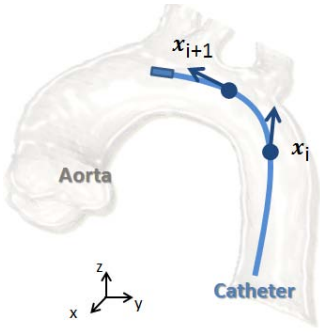

Fig. 1. Approximation of the catheter shape in the pre-operative model reference system. The catheter is represented by a finite number of oriented points $\boldsymbol{x_i}$ connected by a spline.

B. Electromagnetic Catheter Localization and Shape Estimation

A customized catheter with multiple EM sensors has been developed to measure the position and shape in real-time. A 7F (2.33mm) radiofrequency ablation catheter sheath is employed to install small electromagnetic sensors along the catheter length by attaching to the inner sheath of the catheter as depicted in Fig. 2. One 6 Degrees-Of-Freedom (DOF) sensor is positioned at the tip of the catheter in order to estimate the position and the rotation in the three directions. Six 5 DOF sensors are placed at 125 mm intervals except the first sensor which is installed 80mm from the 6 DOF tip sensor in order to have a more accurate shape description near the tip.

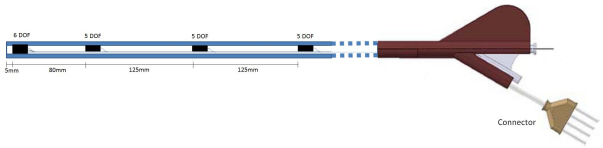

Fig. 2. Customized catheter with multiple EM sensors. A 6 DOF sensor is installed at the catheter tip. Multiple 5 DOF sensors are attached along the catheter length.

Measurement of the catheter position and shape given by the EM tracking system can be expressed as:

$$\boldsymbol{Z}_t = \{\boldsymbol{z}_1, \boldsymbol{z}_2, \ldots, \boldsymbol{z}_n\}_t^T, \tag{2}$$

where $\boldsymbol{z}_i = (x, y, z, \theta, \gamma, \phi)$ is the position and orientation of the i-th sensor in the EM tracking reference system. The initial registration of the pre-operative model and EM tracking is performed before the procedure so as to map the recorded data and the model on the same reference frame. In particular, we assume the global coordinate system as the EM coordinate system and we define the transformation matrix between EM tracking and the pre-operative model as ${}^{E}T_{M}$. In ideal conditions, i.e., with correction of magnetic field distortion and without the presence of ferromagnetic materials, the EM tracking systems can achieve a sub-millimeter localization accuracy. In this situation, the catheter localization would be sufficiently accurate to be used for intraoperative guidance. However, it has been reported [9]

that localization error can increase to 3mm when the sensor is further than 400mm from the field generator. This error is particularly significant considering the possible setup in an operating theater, in which it may not be possible to position the field generator too close to the patient during the entire procedure. Moreover, this approach relies on the fact that no deformation occurred after the registration of the pre-operative model and the EM tracking data. In surgery, small vessel deformation due to respiration and heart beat can introduce errors affecting the visualization of the catheter, which can be represented outside the vessel model causing a reduced reliability of the method by the surgeon.

C. Catheter Insertion Model

The simulation model presented in [8] is used to provide an initial shape estimate of the catheter and its position inside the vessel. This approach relies on the minimization of the bending and elastic energy of the catheter inside the vasculature.

Considering the insertion of the catheter by a length ξ, the displacement of each node $\boldsymbol{x}_i$ of the catheter is given by:

$$\delta \boldsymbol{x}_i = \xi + \sum_{j=0}^{i-1} \boldsymbol{\alpha}_i, \tag{3}$$

with $\boldsymbol{\alpha}_i$ being the displacement vector of the element i-th given the translation of the elements from $(i+1)$-th to n, i.e., the tip of the catheter. The vector $\boldsymbol{\alpha}_i$ can be defined as:

$$\begin{aligned} \boldsymbol{\alpha}_i = &- \frac{a_i^2}{2\lambda}\hat{\boldsymbol{e}}^{(P)} + \frac{a_i}{2\lambda}\sqrt{4\lambda^2 - a_i^2}\cos\psi_i \hat{\boldsymbol{e}}^{(Q)} \\ &+ \frac{a_i}{2\lambda}\sqrt{4\lambda^2 - a_i^2}\sin\psi_i \hat{\boldsymbol{e}}^{(S)}, \end{aligned} \tag{4}$$

where $\{\hat{\boldsymbol{e}}^{(P)}, \hat{\boldsymbol{e}}^{(Q)}, \hat{\boldsymbol{e}}^{(S)}\}$ indicate the 3D Carthesian coordinate system at each node, $a = |\boldsymbol{\alpha}_i|$, λ is the distance between the nodes, i.e. the segment length. In (4), ψ_i is the angle of revolution of the segment around $\hat{\boldsymbol{e}}^{(P)}$. The variables (a_i, ψ_i) for each element i are the two unknowns to be computed to obtain the displacement $\delta \boldsymbol{x}_i$. Therefore, defining the total energy $U_{tot} = U_{bend} + U_{wall}$ as the sum of bending energy U_{bend} of the catheter and the elastic energy of the vessel due to the contact with the catheter U_{wall} the variables (a_i, ψ_i) are obtained by solving the following equations: $\partial U_{tot}/\partial a_i = 0, \forall i$ and $\partial U_{tot}/\partial \psi_i = 0, \forall i$. The bending energy U_{bend} for each joint i is defined according to the Hooke's law and continuous mechanics, such that:

$$U_i^{bend} = \frac{\lambda EI}{2R^2}, \tag{5}$$

where the modulus of the elasticity E, the second moment of area I, the length of the segment λ, and the radius of the catheter R are the parameters that define the mechanical characteristics of the catheter. The vessel elastic energy U_{wall} is defined as the accumulation of contact forces on the wall for each segment given a small displacement $\delta\boldsymbol{\alpha}_i$. A first order iterative analytical solution is proposed to efficiently compute the variables (a_i, ψ_i) and obtain the vector of the displacement of each segment $\delta \boldsymbol{x}_i$.

In the proposed framework, the simulation algorithm is used to predict the catheter position given a certain insertion length ξ. From (3), we can define the vector of all the displacements of the catheter nodes at time t as:

$$\boldsymbol{U}_t = \{\delta \boldsymbol{x}_1, \delta \boldsymbol{x}_2, \ldots, \delta \boldsymbol{x}_n\}_t^T. \tag{6}$$

D. Motion Compensation

During endovascular intervention, vessel motion and deformation make the registration of intra-operative information to a pre-operative model more difficult. Within the proposed framework, a simple but yet effective approach for motion compensation can be provided by exploiting the EM tracking information.

When the catheter is not pushed inside the vessel it is expected to observe no motion of the EM sensors. However, if the catheter is in contact with the vessel walls and motion or deformation occurs in the vasculature, then the EM tracking may report a displacement of the sensors. Therefore, if we define T as the interval in which the deformation is detected we can compute the displacement vector $\boldsymbol{D}_t = \{\boldsymbol{d}_t^i\}_{i=1,\ldots,n}$ as:

$$\boldsymbol{D}_t = \boldsymbol{Z}_t - \boldsymbol{Z}_{t-T}, \tag{7}$$

where $\boldsymbol{d}_t^i = \boldsymbol{z}_t^i - \boldsymbol{z}_{t-T}^i$ provides the translation and rotation for the part of the vessel next to the i-th sensor. Then, a transformation matrix ${}^E T_{M^i}$ can be defined with the rotation and translation information provided by the vector $\boldsymbol{d}_t^i$ to register the deformed pre-operative model to the sensor data coordinate system. It is worth noting that when the deformation can be approximated with a rigid transformation then the transformation matrix ${}^E T_M$ is unique for the whole pre-operative model. This assumption can be realistic for deformations caused by the insertion of a stent graft deployment device. Moreover it has to be pointed out that because of the catheter flexibility the vessel deformation due to the contact is negligible.

E. Probabilistic Fusion Algorithm for Catheter Localization and Motion Prediction

In general, the catheter insertion model presented in Section II-C is able to provide an accurate prediction of the catheter motion and shape given a certain insertion length. The EM-based localization and shape estimation approach described in Section II-B provides a continuous measurement of the catheter position within the vessel. A Kalman Filter is used to fuse these complementary information to provide reliable shape and position estimation during catheter insertion. The diagram of the fusion algorithm is schematically presented in Fig. 3.

The prediction model is defined according to the catheter insertion model. At each time instant, the catheter insertion mechanism is actuated with an insertion length ξ. The catheter displacement can be computed for each segment by using (3) to provide the control variable of the Kalman Filter, for which the transition model of the filter is given by:

$$\boldsymbol{X}_t = A\boldsymbol{X}_{t-1} + B\boldsymbol{U}_t + \omega_t, \tag{8}$$

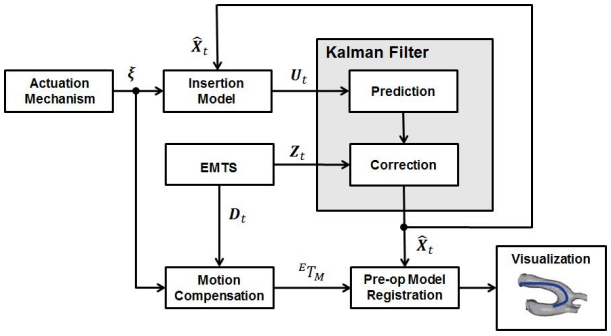

Fig. 3. Diagram of the fusion algorithm

where A and B are identity matrices $I_{n\cdot 6\times n\cdot 6}$ and ω_t is the normally-distributed process noise where $p(\omega_t) = N(0, Q)$, with Q process noise covariance matrix. The process noise is set according to the inaccuracy of the simulation algorithm. The main error of the simulation resides in the difficulty in estimating correctly the friction of the catheter against the vessel walls.

The measurement model is based on the data obtained by the EM tracking system while tracking the sensors attached to the catheter. The observation vector $\boldsymbol{Z}_t$, defined in (2), is obtained as described in Sect. II-B. The measurement model is then represented as:

$$\boldsymbol{Z}_t = H\boldsymbol{X}_t + \nu_t, \tag{9}$$

where H is an identity matrix $I_{n\cdot 6\times n\cdot 6}$ and ν_t is the normally-distributed measurement noise where $p(\nu_t) = N(0, R)$, with R process noise covariance matrix. The noise model is defined to be consistent with the intrinsic errors of the EM tracking system. Following the models definition, the standard Kalman Filter equations provide the estimate of the sensors position $\widehat{\boldsymbol{X}}_t$ and the uncertainty of the localization.

This probabilistic framework has certain advantages for endovascular guidance. They include: 1) the prediction model can be used to estimate in advance the probability of moving the catheter tip and its bends to a potentially dangerous area, as for instance, when it is near an aneurysm or atherosclerotic plaque. The possibility of assessing on a 3D model where the catheter is going to be subsequently to a certain motion can be used to avoid wall hit or vessel perforations. 2) The 3D visualization provides a more intuitive and natural environment for catheter navigation compared to catheter guidance under fluoroscopy. 3) The combination of catheter simulation and EM tracking in a statistical framework compensates for the inaccuracy of the single components in order to obtain a more reliable and accurate localization.

III. RESULTS

A. Experimental Setup

The evaluation of the proposed platform is performed in an *in-vitro* environment using a silicone phantom of the aorta. A 2D phantom has been created by segmenting an MR-scan of a patient using the MIMICS software (Materialise, Leuven, Belgium) as depicted in Fig. 4(a). A projection of the model on a 2D plane has been made and a centerline extracted. The centerline is served as a the basis for the aorta model. The longitudinal thickness of the aorta wall was set to 20mm. The contour of the aorta was cut out from a 3mm thick polycarbonate plate and embedded in a sandwich structure. In our experiments we do not take into consideration the vessel wall deformation as we assumed that the catheter does not change the vessel shape significantly when they are in contact. The phantom is placed on top of the magnetic field generator at approximately 10cm distance.

The camera used to obtain the ground truth images is an Ethernet GigE Prosilica GC650C with a 6mm lens and resolution of 659x493 pixels. The pixel dimension corresponds at approximately 1mm. The camera was placed on a customized mount 720mm above the aorta phantom. To minimize noise and disturbances on the EM measuring system, metal components are avoided and only wood and plastic materials are used to construct the frame that supports the phantom and the camera.

The experiments has been assessed in this 2D setup in order to be able to obtain the ground truth data using a video camera to simulate real-time fluoroscopy and record the catheter insertion. A specialized rig is constructed in order to mount the camera above the phantom with a perpendicular line-of-sight (see Fig. 4(b)). An NDI Aurora EM tracking system (NDI, Ontario, Canada) is used to track the sensor installed in the catheter as described in Section II-B. The EM tracking system was positioned 10 cm below the phantom. The catheter is inserted into the aorta phantom with a constant velocity of 10mm/s by using an actuation mechanism. It is worth noting that a non-constant insertion can be applied since the algorithm in Section II-C can simulate the catheter behavior with different insertion lengths.

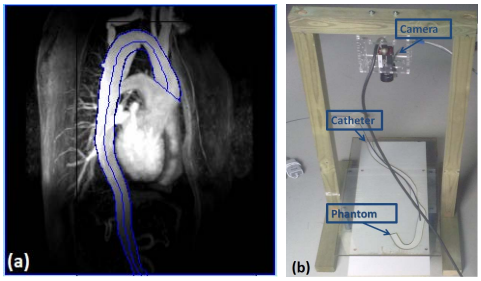

Fig. 4. (a) CT data of the aorta for phantom construction. The blue line indicates the segmentation of the vessel and the correspondent centerline. (b) The experimental setup showing the phantom and the rig with the camera used for the ground truth data generation.

B. Ground Truth Data Generation

The ground truth data for evaluating the accuracy of the localization process is generated using the images acquired with the video camera. An affine transformation is performed to map the image coordinates to the phantom reference system. The transformed image is then processed in order to extract the catheter and compute the sensors positions which

coincide with the correspondent elements of the Kalman Filter state vector $\boldsymbol{X}_t$.

Since the EM sensors are placed inside the catheter sheath, their position is found by computing the distance from the tip along the catheter shape. This is done by processing the images to extract the information required. The first step consists in masking the areas of the image relative to the external part of the phantom in order to isolate the catheter. The catheter shape is obtained by thresholding the image and applying a skeletonization algorithm [10] to obtain the centerline of the catheter. The tip of the catheter is identified in the skeleton by ordering the skeleton points. The positions of the sensors are located according to the distance of the skeleton points from tip. In Fig. 5, the framework for ground truth generation and experiments validation is represented.

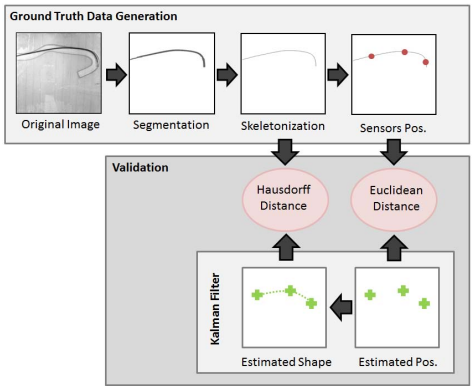

Fig. 5. Ground truth generation and experiments validation. The ground truth of the sensor position and the catheter shape are extracted from the camera image. The estimated position and shape are validated using, respectively, the Euclidean distance and the Hausdorff distance.

C. Experiments

The proposed method has been tested on a 2D phantom by multiple catheter insertions and retractions while acquiring images of the current configuration using the camera. The ground truth has been generated as described in Section III-B. The parameters of the simulation algorithm have been set according to the characteristic of the catheter described in Section II-B. In particular, the radius of the catheter is $R = 2.33mm$, the elasticity is $EI = 2.5 \cdot 10^9 kg/s^2$, and the element length $\lambda = 20mm$. The presented approach has been implemented in C++ and it is compliant with the real-time constraints of the navigation application. The experiments has been performed on an Intel® Core^{TM} i5 650 / 3.2 GHz CPU machine with 4GB RAM.

The tracking approach has been tested by comparing the estimated positions of the sensors to the ground truth. In Fig. III-C the results of the catheter tracking approach during one insertion sequence are provided. The green crosses represent the estimated positions of the sensors while the blue dots are the ground truth locations of the sensors. The red dots are the predicted positions from the previous instant. The results and the ground truth sensor positions are registered and superimposed to the acquired camera image. It can be noticed that the position estimation is accurate and it can be used to approximate the catheter shape.

In Table I the quantitative results of the accuracy of the method is shown comparing the presented approach with the localization obtained by using only the EM tracking and only the insertion model. It can be observed that the fusion algorithm improves the localization accuracy for the three sensors by effectively integrating the complementary information of the EM tracker and of the insertion model.

TABLE I

AVERAGE POSITION ERROR COMPUTED ON 20 CATHETER POSES. S1 INDICATES THE SENSOR AT THE CATHETER TIP, S2 THE SENSOR IN THE MIDDLE, AND S3 THE SENSOR CLOSER TO THE CATHETER DISTAL END.

Sensor	EM Tracking	Insertion Model	Fusion
S1	2.5mm	3.0mm	1.8mm
S2	2.9mm	3.4mm	2.1mm
S3	3.5mm	3.2mm	2.3mm
$\forall$ S	3.0mm	3.2mm	2.1mm

The accuracy of the shape estimation is tested by computing the Hausdorff distance between the spline connecting the points $\boldsymbol{X}_t$ and the skeleton of the catheter captured from the camera. The Hausdorff distance is a metric widely used to compare trajectories represented as sets of points in a metric space. If we consider two sets of points $S = \{s_1, s_2, \ldots, s_m\}$ and $T = \{t_1, t_2, \ldots, t_n\}$, the Hausdorff distance is defined as:

$$d_{HD} = \min(h(S,T), h(T,S)), \tag{10}$$

where $h(S,T) = \max_{s \in S} \min_{t \in T} d(s,t)$ and $h(T,S) = \max_{t \in T} \min_{s \in S} d(t,s)$ with $d(s,t)$ as the Euclidean distance between a point $s \in S$ and $t \in T$. In Fig. 7, another set of 20 catheter shapes have been estimated at different positions within the phantom.

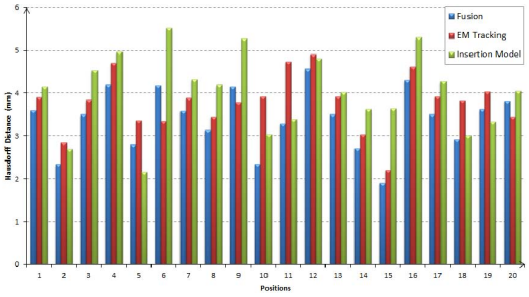

Fig. 7. Graph of the shape estimation error. The Hausdorff distance between the estimated shape and the ground truth is reported for the following approaches: 1) only EM localization; 2) only insertion model; 3) proposed fusion algorithm.

The shape estimation obtained using only the EM sensors information, the shape provided by the simulation algorithm, and the one resulting from the fusion algorithm are compared to show improved accuracy of the proposed method.

In Fig. 8, an example of the motion compensation approach is shown. The phantom has been shifted of 4mm in the x direction and 10mm in the y direction while the catheter was not pushed by the catheter inserter. The

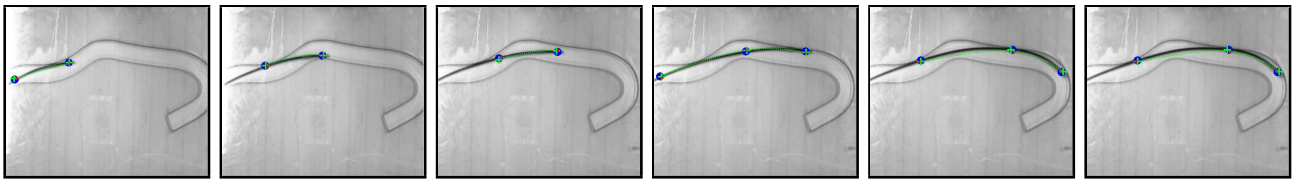

Fig. 6. Tracking experiments on 6 catheter poses of a continuous insertions sequence. The ground truth position of the sensors is indicated by a blue dot. The estimated position resulting from the fusion algorithm is depicted as a green cross. The dotted line is a spline that connects the estimated positions. The red dots represent the prediction of the catheter position from the previous frame.

displacement vector $\boldsymbol{D}_t$ is obtained from the EM tracking system and transformation matrix ${}^{E}T_{M}$ representing the translation is computed accordingly. In Fig. 8(a) the visual artifact introduced by the shift is shown. In Fig. 8(b) the motion compensation approach corrects the registration and provides a reliable result.

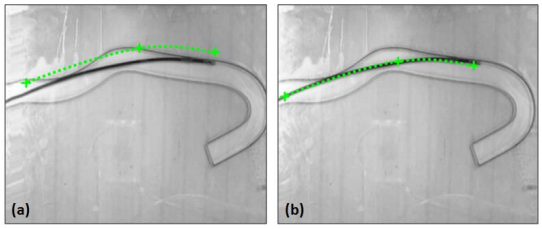

Fig. 8. Motion compensation example. The phantom has been shifted of 4mm and 10mm in x and y direction respectively while the catheter actuator does not move the catheter. (a) Catheter localization obtained with the fusion algorithm after the translation; (b) The results of the localization after applying the motion compensation method.

Finally, an example of the improved visualization provided by the proposed algorithm is shown in Fig. 9 where the catheter estimated position within a phantom of the aorta is visualized in a 3D graphical environment. The result is obtained by inserting the catheter in an Elastrat (Elastrat Sarl, Geneva, Switzerland) pulsatile silicone phantom of the aortic arch (200x175x125 mm) and by representing the catheter through the interpolation of the EM detected position by cubic Hermite splines.

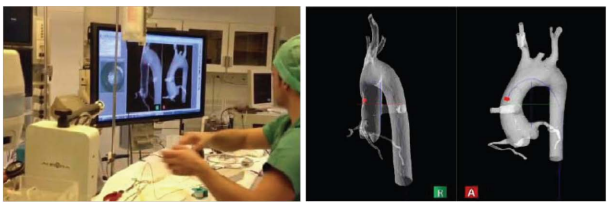

Fig. 9. The experimental setup for the 3D shape estimation and the 3D visualization of the catheter shape estimated using EM sensors position along the catheter length (the red dot indicates the tip of the catheter).

IV. CONCLUSIONS

In this paper we have proposed a novel method for catheter navigation based on the combination of insertion simulation and EM tracking. A customized catheter with multiple EM sensors displaced along its length has been developed in order to measure the position and assess the shape. The insertion simulation algorithm is used to provide a prediction of the catheter dynamic consequent to a certain insertion length. A novel framework based on a Kalman Filter is presented to support the surgeon during the intervention by providing catheter position and shape estimation. To the best of our knowledge this is the first work integrating catheter motion computer simulation and EM-based catheter shape estimation for robotically assisted catheter navigation. The experiments show the reliability of the method and the potential to improve the safety catheter procedures by reducing the use of fluoroscopy, allowing the visualization of the catheter, and predicting catheter motion. Future works will be devoted to the extension of the approach to 3D.

REFERENCES

[1] J. Jayender, R. V. Patel, G. F. Michaud, and N. Hata, "Optimal transseptal puncture location for robot-assisted left atrial catheter ablation," in *Proceedings of the 12th International Conference on Medical Image Computing and Computer-Assisted Intervention: Part I, MICCAI 2009*, 2009, pp. 1–8.

[2] P. Wang, T. Chen, O. Ecabert, S. Prummer, M. Ostermeier, and D. Comaniciu, "Image-based device tracking for the co-registration of angiography and intravascular ultrasound images," in *Proceedings of the 14th International Conference on Medical Image Computing and Computer-Assisted Intervention, MICCAI 2011*, Sept. 2011, pp. 161–168.

[3] A. Dore, S.-L. Lee, and G.-Z. Yang, "Probabilistic localization of catheter tip from ivus images," in *The MICCAI Workshop on Computing and Visualization for (Intra)Vascular Imaging (CVII)*, Sept. 2011.

[4] C. Shi, C. Tercero, S. Ikeda, T. Fukuda, K. Komori, and K. Yamamoto, "In-vitro three dimensional vasculature modeling based on sensor fusion between intravascular ultrasound and magnetic tracker," in *IEEE/RSJ International Conference on Intelligent Robots and Systems*, Sept. 2011, pp. 2115–2120.

[5] S. B. Salomon, T. Dickfield, and H. Calkins, "Real-time cardiac catheter navigation on three-dimensional ct images," *J. Interv. Card. Electr.*, vol. 8, pp. 27–36, 2003.

[6] J. Wang, T. Ohya, H. Liao, I. Sakuma, T. Wang, I. Tohnai, and T. Iwai, "Intravascular catheter navigation using path planning and virtual visual feedback for oral cancer treatment," *International Journal of Medical Robotics and Computer Assisted Surgery*, vol. 7, no. 2, pp. 214–224, 2011.

[7] A. M. Okamura, K. T. Ramesh, B. W. Schafer, K. B. Reed, and S. Misra, "Observations and models for needle-tissue interactions," in *Proc. of the IEEE International Conference on Robotics and Automation, ICRA 2009*, Kobe, Japan, 2009, pp. 2687–2692.

[8] M. K. Konings, E. B. van de Kraats, T. Alderliesten, and W. J. Niessen, "Analytical guide wire motion algorithm for simulation of endovascular interventions," *Medical and Biological Engineering and Computing*, vol. 41, pp. 689–700, 2003.

[9] H. Fontenelle, R. Palomar, and O. J. Elle, "On the use of electromagnetic tracking systems for catheter tracking in image guided surgery," in *2nd National Ph.D. Conference in Medical Imaging and the Annual MedViz Conference*, Jan. 2011.

[10] T. Y. Zhang and C. Y. Suen, "A fast parallel algorithm for thinning digital patterns," *Communications of the ACM*, vol. 27, no. 3, pp. 236–239, 1984.